Journal of Materials Chemistry A

ROYAL SOCIETY OF CHEMISTRY

PAPER

View Article Online
View Journal | View Issue

Cite this: J. Mater. Chem. A, 2024, 12, 20121

Imine-based covalent organic framework gels for efficient removal of Fe^{2+} from contaminated water†

Cristina Arqueros,[ab] Lorena Welte,[a] Carmen Montoro *[bc] and Félix Zamora *[bd]

The presence of high concentrations of metal ions in water distribution systems and industrial plants gives rise to the appearance of deposits responsible for incrustation and corrosion events. In this context, the search for new approaches to remove these contaminants from water using more efficient techniques has gained substantial importance over the last decades. Covalent Organic Frameworks (COFs) have emerged as a new class of porous crystalline materials with distinctive properties based on the reticular chemistry principle, making them very promising for this purpose. Specifically, they are characterized by their permanent porosity, excellent water stability, and tailored design for specific applications on demand. In this study, we present two imine-based COFs, **TAPB-PDA-COF** and **TAPB-DHTA-COF**, obtained at room temperature, as a sustainable alternative for the removal of Fe^{2+} from water as a previous step to reverse osmosis in the water treatment process. The two imine-based COFs were directly obtained as gels and easily activated under argon flow to xerogels. The materials showed remarkable adsorption uptakes at neutral pH towards Fe^{2+} within 5 minutes of contact. Additionally, the COF xerogels exhibited maximum adsorption capacity values in the range of other porous reported materials. Finally, the gels were successfully processed into COF@Polysulfone composite beads, paving the way for the obtention of COFs into macroscopic products easily removable from any media, leaving no residues, and easily incorporated into the water treatment process. These COF composite beads are excellent candidates for large-scale preparation and easy commercialization.

Received 9th February 2024
Accepted 25th June 2024

DOI: 10.1039/d4ta00954a

rsc.li/materials-a

Introduction

Water is an essential resource for life and, in general, for our planet. Indeed, about 71% of the Earth's surface is covered by water, while the remaining 29% consists of continents and islands. The oceans hold approximately 96.5% of Earth's water, while only 3.5% is freshwater.[1] However, it is estimated that 99% of terrestrial water cannot be used, and less than 1% is available for human and animal consumption. Due to its ability to dissolve nearly any substance, natural water contains dissolved minerals, inorganic and organic substances, gases, and even microorganisms, so it is impossible to use directly. This fact and its increasing scarcity make the availability of good-quality water a worldwide problem. It is necessary to address effective water treatment processes to ensure they meet the standard quality parameters.[2] Some contaminants that must be removed from water are metal ions because they are toxic to humans and contribute to the deterioration of water distribution systems and industrial plants.[3] Iron is one of the metal ions that cause more corrosion and scaling problems due to the formation of deposits. It exists predominantly as ferric iron (Fe^{3+}) in oxygenated environments due to its quick oxidation from ferrous iron (Fe^{2+}) when exposed to dissolved oxygen or air. Fe^{3+} forms solid precipitates, often as iron oxyhydroxides, resulting in reddish-brown sediments or water discoloration.[4] Anthropogenic sources of iron that contribute to its discharge into natural water sources include industries such as mining, steel production, metal plating, metal fabrication, battery, and chemical manufacturing. The European regulation by Directive EU 2020/2184 (ref. 5) establishes the maximum allowable concentration of iron in water to be safe for human consumption in 0.2 mg L^{-1}. The average concentration of this metal in rivers has been reported to be 0.7 mg L^{-1}, and in anaerobic groundwater, in the form of Fe^{2+}, ranges between 0.5 and 10 mg L^{-1}.[6] High concentrations of iron in drinking water entails severe health risks, including gastrointestinal issues, nutrient absorption interference, and hemochromatosis.

Several water treatment processes commonly used to remove iron include oxidation, filtration, coagulation, flocculation *via*

[a]Kleinscale, Avenida Ciudad de Valencia S/N Parque Comercial Vera Plaza, Vera-Playa, 04621, Almería, Spain
[b]Departamento de Química Inorgánica, Facultad de Ciencias, Universidad Autónoma de Madrid, 28049 Madrid, Spain. E-mail: felix.zamora@uam.es; carmen.montoro@uam.es
[c]Institute for Advanced Research in Chemical Sciences (IAdChem), Universidad Autónoma de Madrid, 28049 Madrid, Spain
[d]Condensed Matter Physics Center (IFIMAC), Universidad Autónoma de Madrid, Madrid, 28049, Spain

† Electronic supplementary information (ESI) available. See DOI: https://doi.org/10.1039/d4ta00954a

chemical precipitation, ion exchange, and reverse osmosis. Oxidation/filtration involves converting Fe^{2+} to Fe^{3+} through agents like chlorine, potassium permanganate, or air, followed by filtration. Coagulation/flocculation requires pH adjustment and the addition of chemicals (*e.g.*, ferric chloride, ferric sulphate, or poly aluminium chloride coagulants) to promote particle aggregation, followed by sedimentation or filtration for the final removal. These methods are easy and *a priori* affordable. However, in most cases, adding these flocculants enhances and promotes the generation of sludges containing high concentrations of aluminium, iron, and organic matter that are harmful to the environment, leading to extra operational costs of sludge disposal.[7,8]

Hence, developing porous materials capable of selectively interacting through adsorption processes with iron present in water is necessary to improve current decontamination technologies. In this sense, reticular materials such as metal–organic frameworks (MOFs) and covalent organic frameworks (COFs) appear promising candidates for this purpose.[9,10] The advantage of this kind of materials, compared to classical porous materials, such as adsorbed coal and zeolites, lies in the rational design of their structures. This means that the topology and features of their pores can be modulated by choosing the molecular building blocks or introducing functional groups, either pre- or post-synthetically. Then, structures with different properties can be prepared to carry out efficient and selective capture, in this case, of molecules and ions present in water. The main difference between both crystalline materials is related to their stability in water since, in the case of MOFs, it is limited. In contrast, COFs show significant stability in acidic and basic aqueous media and are metal-free, avoiding leaching problems and making them advantageous candidates for water treatment.[11] Among the different linkages reported by COFs, those based on imine bonds are the most explored since their introduction in 2009.[12] Imine-based COFs are obtained *via* condensation of a primary amine and an aldehyde, which is an easily accessible reaction due to the wide variety of monomers available. These dynamic bonds, however robust, offer good thermal and chemical stability to the frameworks.[13] Indeed, they have been extensively studied in capturing and detecting contaminants present in water, such as pharmaceuticals,[14–17] dyes,[18,19] and metal ions.[20–22] For example, in 2017, Merí-Bofí *et al.* prepared a thiol-grafted imine-based COF *via* post-synthetic functionalization with a click reaction. The material showed exceptional removal rates towards Hg^{2+} in water, with the largest adsorption capacity reported for this ion, 4395 mg g^{-1}.[23] Lu and co-workers synthesized a carboxy-functionalized COF to remove Pb^{2+} in water, achieving uptake rates above 90% even after 20 cycles.[24] The same year, a triazine COF with hydroxy bifunctional groups prepared by Xu *et al.* was reported for the removal of the same ion. The removal efficiency reached 99% within 5 minutes of contact. The large chelating sites in the pores derived from the hydroxyl groups were responsible for one of the largest adsorption capacities obtained towards Pb^{2+} in water.[25] Apart from heavy metal ions, not much has been reported concerning the application of COFs towards removing metal ions responsible for incrustation and corrosion events in industrial plants.

The COF processability is another crucial aspect to consider when establishing their final application.[26] In this sense, most COFs are obtained as polycrystalline solids, which cannot be implemented under continuous flow conditions. Therefore, exploring alternatives for incorporating COF materials into conventional filtration systems or developing new ones is essential.[27] In this regard, our group has made significant progress in that field since we have been able to prepare them in the form of nanoparticles,[20] aerogel monoliths,[28] free-standing membranes,[29] and even in the form of inks for 3D-printing applications.[30]

In light of these considerations, we have selected two chemically robust imine-based COFs that can be directly prepared as gels and easily transformed into xerogels. In addition, we have explored the feasibility of using these materials in water treatment applications, specifically for Fe^{2+} capture in water media, as an environmentally respectful alternative. Also, the materials have been successfully processed into COF composite beads mixed with a non-porous polymer, polysulfone, to afford a direct product, enabling the implementation of the materials in the treatment of industrial water. The procedure to produce COF composite beads is straightforward for a large-scale and commercialized preparation.

Results and discussion

Synthesis and characterization of COFs

Two imine-based COFs were selected for the removal of Fe^{2+} from water. Both materials were prepared following procedures previously reported with slight modifications.[28,31] Special attention has been paid to obtaining them under environmentally sustainable conditions, utilizing green solvents, and conducting synthesis at room temperature. In particular, compared with other methods that require unfavourable energetic conditions,[32–34] our approach enables the preparation of COF gels at room temperature, representing significant energy savings. Then, after the Schiff condensation reaction at room temperature of 1,3,5-tris-(4-aminophenyl)benzene (TAPB) with terephthalaldehyde (PDA) or 2,5-dihydroxybenzene-1,4-dicarboxaldehyde (DHTA) (2 : 3 molar ratio) we obtained the COF gels (GCOF) **TAPB-PDA-GCOF** and **TAPB-DHTA-GCOF**, respectively (Scheme 1). Briefly, for the preparation of **TAPB-PDA-GCOF**, TAPB, and PDA were dissolved separately in acetic acid (AcOH): 10% H_2O. A bright red gel formed instantly after adding the aldehyde over the amine. For the preparation of **TAPB-DHTA-GCOF**, TAPB, and DHTA were dissolved in a 4 : 1 *p*-dioxane : mesitylene solution. Then, 10.5 M AcOH was added, and an orange gel was rapidly formed. Both gels were left undisturbed for 3 days at room temperature to improve their crystallinity and porosity properties. The activation through solvent exchanges with tetrahydrofuran (THF) and ethanol (EtOH) followed by Ar flow-drying in the first case and supercritical CO_2 ($scCO_2$) for the second case yield the materials in the form of xerogels (**TAPB-PDA-COF** and **TAPB-DHTA-COF**). As

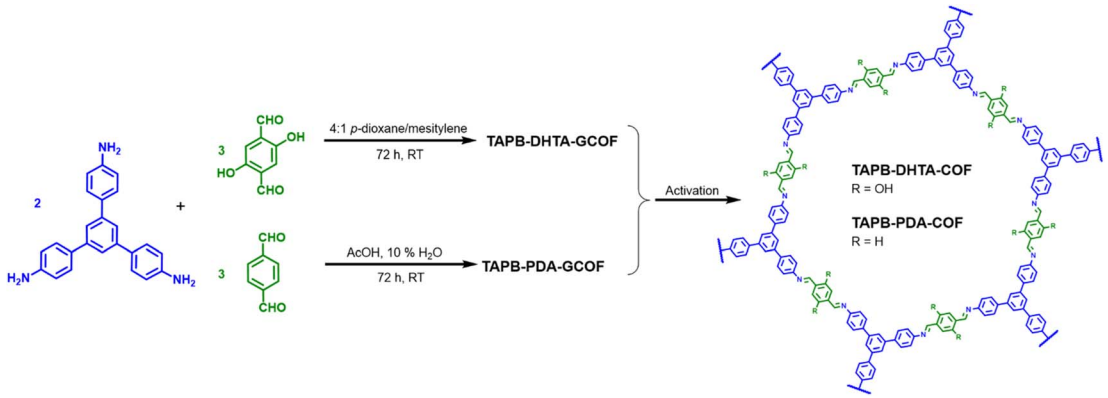

Scheme 1 Scheme of the synthetic procedure for TAPB-PDA-COF and TAPB-DHTA-COF in the form of gels and xerogels.

confirmed previously, **TAPB-DHTA-COF** requires a softness activation process to avoid the gel structure collapse.[31]

It is highlighted that the structural, morphological, and textural characterization was carried out after the activation of the COF gels, which means for the xerogels **TAPB-PDA-COF** and **TAPB-DHTA-COF**.

The correct formation of the imine linkage for both frameworks was corroborated by Fourier-transform infrared spectroscopy (FTIR) and solid-state ^{13}C cross-polarization magic angle spinning nuclear magnetic resonance (^{13}C CP-MAS NMR). FTIR spectra of both materials showed the imine bond (–C═N) at around 1600 cm^{-1}, confirming the obtention of the imine linkage (Fig. S4.1 from ESI†). The absence of the carbonyl signal (C═O) of each aldehyde, PDA, or DHTA, at 1684 and 1664 cm^{-1}, respectively, as well as the peaks of the ν(N–H) from the TAPB in the COF spectra, proved the complete condensation between the building blocks. They left no remaining unreacted monomers in the final product. ^{13}C CP-MAS NMR spectra also corroborated the formation of the imine bonds in the materials. The signals corresponding to the C sp^2 appeared at chemical shifts between 121 and 145 ppm (see S5.1 from ESI†). The carbon linked to the hydroxy group displayed a chemical shift at 153 ppm (j) in the **TAPB-DHTA-COF** spectra. The crystallinity of the materials was studied by powder X-ray diffraction (PXRD). Diffraction patterns of **TAPB-PDA-COF** and **TAPB-DHTA-COF** confirmed that both materials were obtained with high crystallinity (Fig. S3.1 from ESI†), presenting the signals at 2θ = 2.83°, 4.90°, 5.63°, 7.45°, corresponding to the 100, 110, 200, 210 diffraction peaks. The experimental data collected successfully matched the simulated patterns. Thermal gravimetric analyses (TGA) revealed high thermal stability for both materials. **TAPB-PDA-COF** was stable thermally over 500 °C and **TAPB-DHTA-COF**, around 450 °C (see S8 Section from ESI†).

The porosity of both materials was evaluated by the measurements of N_2 adsorption–desorption isotherms at 77 K. The isotherms were adjusted to the Brunauer–Emmett–Teller (BET) to calculate the specific surface area. In contrast, the pore size distribution (PSD) was calculated based on the non-local density functional theory (NLDFT) (see S9 from ESI†). Both COFs showed Type I and II isotherms, with large BET surface areas, 1450 $m^2\ g^{-1}$ and 1150 $m^2\ g^{-1}$ for **TAPB-PDA-COF** and **TAPB-DHTA-COF**, respectively. Finally, the PSD revealed an average pore size of 3.36 nm and 3.22 nm for **TAPB-PDA-COF** and **TAPB-DHTA-COF**, respectively. As expected, the specific surface area and pore size for **TAPB-DHTA-COF** were slightly smaller than for **TAPB-PDA-COF** due to the pendant hydroxy groups in the pore. Scanning Electron Microscopy (SEM) assessed the morphology of both materials. SEM images revealed that **TAPB-PDA-COF** showed a leaf-like morphology. In contrast, **TAPB-DHTA-COF** possessed a sponge-like granular morphology, where the particles formed larger aggregates (Fig. 1). Given the success in preparing the materials, we decided to test their performance in capturing Fe^{2+} from contaminated waters. The results of the studies on the adsorption properties of COFs in xerogel form are shown below.

Additionally, the COF gels were processed as composites also to evaluate their Fe^{2+} capture properties in water. The advantage of using this type of system is that it can be easily incorporated

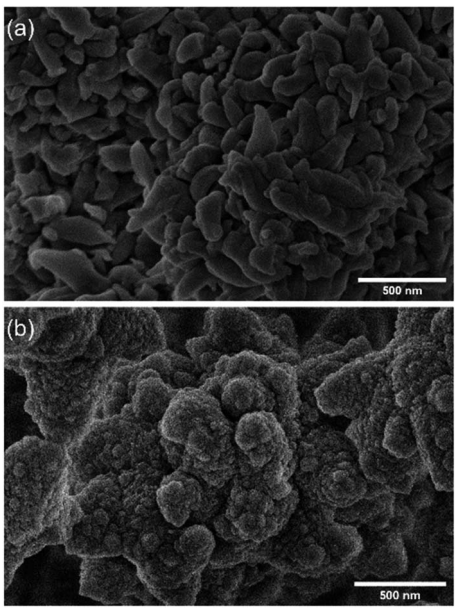

Fig. 1 SEM images of (a) TAPB-PDA-COF and (b) TAPB-DTHA-COF.

at any stage of the water treatment process; it is easily removable and leaves no residues. This approach was carried out considering an emerging processing methodology involving the encapsulation of porous materials within a non-porous polymer matrix through spherification to produce composite beads.[35] Beads of the COF@Polymer composite were obtained following a reported procedure.[36] Briefly, the COF gels were solvent-exchanged with NMP, filtered through filter paper, and suspended in a 10 wt% PSU/NMP solution. Beads were prepared with a 20 wt% loading of COF in the PSU polymer (Section S2 in ESI†). The successful obtention of the composite beads, **TAPB-PDA-COF@PSU** and **TAPB-DHTA-COF@PSU**, was corroborated *via* FTIR. The presence of the (C=N) signal corresponding to the imine bond in the beads' spectra confirmed the correct incorporation of the COF in the polymer matrix (Fig. S4.2 and S4.3 in ESI†). Beads exhibited mean diameter sizes between 2–2.5 mm. N_2 adsorption–desorption isotherms of the prepared beads revealed the formation of new pores within the composite beads (Fig. S9.3 and S9.4 in ESI†). Additionally, the polymeric polysulfone matrix has high chemical stability in the pH range of 2 to 13, and it is resistant to mineral acids, alkalis, and oxidizing agents.[37] Widening the operational range of the COF@PSU composite beads in different aqueous media, ideal in wastewater treatment applications.

Adsorption capability

Firstly, we performed an initial test to check the capacity of the COFs against our target pollutant. For it, **TAPB-PDA-COF** and **TAPB-DTHA-COF** were placed in 15 mL of a 1 ppm Fe^{2+} solution with pH 7 and stirring for 1 h. Then, the samples were filtered, and the final Fe^{2+} concentration was measured by Inductively Coupled Plasma-Mass Spectrometry (ICP-MS). Adsorption capacity (Q_e) was calculated with the following equation:

$$Q_e = \frac{(C_i - C_f)\cdot V}{m} \quad (1)$$

where C_f (mg L^{-1}) is the final concentration of the liquid phase, C_i (mg L^{-1}) is the initial concentration, V (L) is the sample volume, and m (g) is the mass of the adsorbent.

The results initially showed 78% and 81% retention rates for **TAPB-PDA-COF** and **TAPB-DHTA-COF**, respectively. Subsequently, PXRD and SEM microscopy measurements were carried out to evaluate the robustness of the xerogel COFs under experimental conditions. The analyses confirmed the materials retained their crystalline structure and morphology (Fig. S3.2 and S7.1 from ESI†). So, further studies were performed to investigate the adsorption properties of both materials.

pH dependence studies

The pH of the sample can have an impact not only on the surface charge of the adsorbent but also on the specific metal ion species present. This fact directly affects the nature and strength of the interaction between them. The pH dependence studies were conducted using five water samples containing 1 ppm Fe^{2+} at different pH values: 3, 5, 8, 10, and 11. The pH of the solutions was adjusted using 0.1 mol L^{-1} NaOH and 0.1 mol L^{-1} HCl solutions. Then, around 10 mg of each COF xerogel was put in contact with 15 mL of the sample for 1 h and under stirring at 200 rpm. Finally, the solutions were filtered to remove the COF, and the final concentration was measured *via* ICP-MS.

It was found that the adsorption capacity of **TAPB-PDA-COF** showed a maximum at pH 8, decreasing drastically at higher pH values. Something similar happened for the **TAPB-DHTA-COF**; the adsorption capacity towards iron increased with the pH, reaching its maximum at pH 8, and then slightly decreasing at higher pH. As the pH increased, it was expected that the negatively charged surface of the adsorbent would promote electrostatic interactions between the COF and the ion (Fig. 2). A decrease in the pH would lead to a more significant presence of H_3O^+ ions, causing protonation of the hydroxy groups and thereby inducing electrostatic repulsion toward Fe^{2+} ions, ultimately decreasing the adsorption capacity.

Adsorption isotherms

Adsorption isotherms play a crucial role in predicting the mechanism and performance of adsorption processes. These studies are conducted under constant conditions of temperature and pH, only varying the initial pollutant concentration. In this case, **TAPB-PDA-COF** and **TAPB-DTHA-COF** adsorption capacity was assessed by mixing 10 mg of the material in contact with aqueous solutions of Fe^{2+} (0–5 mg L^{-1}). The samples were shaken at 200 rpm for one hour at 298 K. After that, the solution was filtered to remove the COF and the final concentration was measured.

There are numerous adsorption models, such as the Langmuir, Freundlich, Dubinin–Radushkevich, Henry, Temkin, *etc*, that have been developed to analyze the experimental data and predict the nature of adsorption (monolayer, multilayers, or homogeneous/heterogeneous). In this case, the experimental adsorption results were fitted to a Langmuir isotherm model (see S10 Section from ESI†). This model assumes the formation of a homogeneous monolayer of adsorbate on the material's surface. Once all these active sites become occupied by ions, no

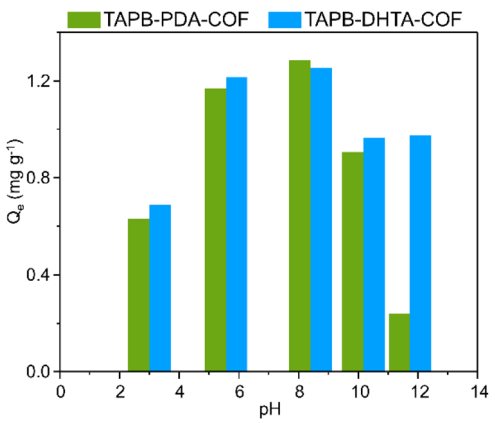

Fig. 2 Q_e of TAPB-PDA-COF and TAPB-DTHA-COF towards Fe^{2+} depending on the pH of the media.

additional adsorption onto the surface occurs. This isotherm is expressed with the following mathematical equations:[38,39]

Non-linear equation:

$$Q_e = Q_{max} \cdot \frac{C_e \cdot K}{(1 + K \cdot C_e)} \quad (2)$$

where Q_e (mg g^{-1}) is the quantity adsorbed in the equilibrium C_e (mg L^{-1}) is the equilibrium concentration of the liquid phase, K (L mg^{-1}) is the Langmuir affinity constant, and Q_{max} (mg g^{-1}) is the maximum capacity of the adsorbent.

Eqn (2) can be linearized as eqn (3) by plotting C_e/Q_e against C_e to calculate the Langmuir isotherm parameters.

Linear form:

$$\frac{C_e}{Q_e} = \frac{1}{K \cdot Q_{max}} + \frac{1}{Q_{max}} \cdot C_e \quad (3)$$

The maximum adsorption capacity (Q_{max}) of the xerogels was calculated with eqn (3), resulting in Q_{max} = 7.3 mg g^{-1} and 8.8 mg g^{-1} for **TAPB-PDA-COF** and **TAPB-DTHA-COF**, respectively (Fig. 3b).

The adsorption properties of the gels (**TAPB-PDA-GCOF** or **TAPB-DTHA-GCOF**) were also tested in iron removal. After the solvent was exchanged with THF and EtOH, the solvent was exchanged with distilled water instead of drying the gels. Four water exchanges were performed to remove the EtOH from the pores and afford the GCOFs. They were placed in 10 mL of a solution containing 1 ppm Fe^{2+} for 1 hour. The adsorption capacity was calculated considering the theoretical mass of the product, assuming a 95% yield.

Although the GCOFs showed poorer adsorption capacities than the xerogel, they exhibited substantial retention rates (Table 1). These results suggest that the gels possess significant retention properties towards Fe^{2+}, enabling a more comprehensive range of potential processing approaches using a more straightforward procedure.

The adsorption capacity of the composite beads towards Fe^{2+} was tested using a 0.65 ppm solution. 25 mg of the composite beads were weighed and mixed with the Fe^{2+} water solution for 1 hour. Then, the beads were separated, and the iron concentration was measured before and after the treatment. Q_e was calculated considering that the COF mass represents only 20 wt% of the total mass:

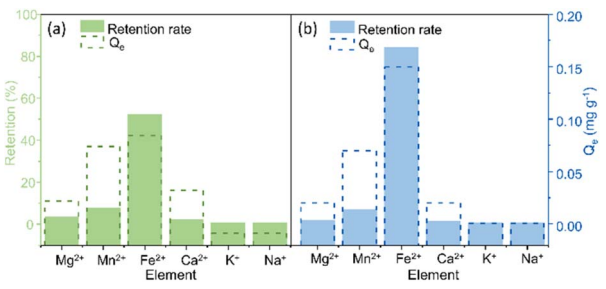

Fig. 3 Adsorption selectivity test of (a) TAPB-PDA-COF, and (b) TAPB-DHTA-COF in the presence of other cations: Ca^{2+}, Mg^{2+}, Mn^{2+}, Na^+, Fe^{2+}, and, K^+. C_{Ca} = 1.715 ppm, C_{Mg} = 0.982 ppm, C_{Mn} = 1.095 ppm, C_{Na} = 0.376 ppm, C_{Fe} = 0.177 ppm, and C_K = 0.283 ppb.

$$m_{COF} = \frac{m_{beads} \cdot wt\%}{100} \quad (4)$$

where m_{beads} (mg) is the total mass of the beads, wt% is the weight loading of COF compared to PSU, and m_{COF} (mg) is the total mass of COF in the beads used.

Results on the adsorption performance of **TAPB-PDA-COF@PSU** and **TAPB-DHTA-COF@PSU** showed the beads removed around 24–28% of the Fe^{2+} concentration in the sample (Table 1). The retention rates and adsorption capacity achieved with the COF composite beads were lower than those of the COF xerogels or the gels. Nevertheless, with further investigations into this procedure, these results exhibit a substantial premise and lay the groundwork for incorporating COFs into water treatment processes.

These values of the assayed materials in the form of gel, xerogel, and composite beads were compared to other recently reported sorbents for removing Fe^{2+}. Compared to several activated carbons – granular activated carbon (3.6 mg g^{-1}),[40] and activated carbons derived from agro-residues (0.8 mg g^{-1})[41] – both of our materials show larger adsorption capacities. We have also compared these results with other materials, such as zeolites (1.1 mg g^{-1})[42] or iron oxide-coated microspheres (2.6 mg g^{-1}).[43] Our results are only surpassed by three reported materials: adsorbent coal (15 mg g^{-1}),[44] bentonite (64.94 mg g^{-1}),[45] and magnetic graphene oxide (MGO) (43.2 mg g^{-1}).[46] However, only MGO showed faster kinetics, 1 minute for saturation, than our materials, 5 minutes (Table S10.7 from ESI†). Only one COF-based derivate was found in the bibliography for comparison.[47] This polydopamine-modified COF, COF@PDA, obtained under inert solvothermal conditions, exhibited large Q_{max} (204.9 mg g^{-1}) and fast kinetics. Nevertheless, our materials were obtained at room temperature, and we were able to process them under continuous flow conditions. This translates into increased energy and cost efficiency, resulting in a more environmentally friendly approach.

Adsorption kinetics

Additionally, the adsorptive properties of the xerogels were studied at different contact times to study the kinetics. This allowed us to determine the minimum time needed to reach the saturation concentration and the efficiency of the materials.

The experiments were carried out by putting 10 mg of **TAPB-PDA-COF** or **TAPB-DTHA-COF** in contact with 15 mL of an aqueous 1 ppm Fe^{2+} solution (see S10 Section from ESI†). The samples were shaken at 200 rpm, with only varying contact times (t = 5, 10, 15, 30, 60, and 240 min).

The adsorption rate of metal ions at low concentrations in water is usually studied using pseudo-second-order kinetics.[48] The pseudo-second-order kinetic model is described with the following equations:[38]

Non-linear equation:

$$Q_t = \frac{k_2 \cdot Q_e^2 \cdot t}{(1 + k_2 \cdot Q_e \cdot t)} \quad (5)$$

Linear form:

Table 1 Adsorption results of the COFs in the form of xerogels, gels, and COF@PSU composite beads under the same operating conditions. Experimental conditions $T = 298$ K, salt: $FeCl_2 \cdot 4H_2O$, $t = 1$ h, $V_{(\text{xerogel COFs})} = 15$ mL, $V_{(\text{GCOFs and composite beads})} = 10$ mL

Sample	m (mg)	C_i (mg L^{-1})	C_f (mg L^{-1})	R (%)	Q_e (mg g^{-1})
TAPB-PDA-COF	10.4	0.89	0.01	99	1.27
TAPB-DHTA-COF	10.5	0.89	0.01	99	1.26
TAPB-PDA-GCOF	10.1	0.99	0.45	55	0.54
TAPB-DHTA-GCOF	10.5	0.99	0.51	48	0.46
TAPB-PDA-COF@PSU	25.5	0.65	0.47	28	0.35
TAPB-DHTA-COF@PSU	24.7	0.65	0.50	24	0.31

$$\frac{t}{Q_t} = \frac{1}{k_2 \cdot Q_e^{\,2}} + \frac{1}{Q_e} \cdot t \quad (6)$$

where Q_t (mg g^{-1}) is the quantity adsorbed at a determined t (min), and Q_e (mg g^{-1}) is the quantity adsorbed at equilibrium. k_2 (g min^{-1} mg^{-1}) is the pseudo-second-order rate constant.

Adsorption kinetics revealed the adsorption capacity (Q_t) rapidly reached 80% uptake for **TAPB-PDA-COF** and 75% adsorption rate for **TAPB-DHTA-COF** within five minutes. In order to corroborate the accuracy and reproducibility of the results, measurements were performed in triplicate (Tables S10.5 and S10.6†). The resulting data were fitted to a pseudo-second-order kinetic model ($r_{\text{TAPB-PDA-COF}}^{\,2} = 0.99988$ and $r_{\text{TAPB-DHTA-COF}}^{\,2} = 0.99995$), and the pseudo-second-order rate constant (k_2) was obtained from the linear equations using eqn (6), $k_{2\ \text{TAPB-PDA-COF}} = 0.596$ g min^{-1} mg^{-1} and $k_{2\ \text{TAPB-DHTA-COF}} = 0.553$ g min^{-1} mg^{-1} (Fig. S10.2 and S10.3, ESI†). This indicates that the COFs and adsorbate interaction occurs quickly at low concentrations.

Selectivity test

A selectivity test was performed using a solution containing a mixture of Mg^{2+}, Mn^{2+}, Fe^{2+}, Ca^{2+}, K^+, and Na^+ to assess the interfering effect of other elements. The selectivity study used 10 mL of solution with 10 mg of each COF xerogel. For **TAPB-PDA-COF** (Fig. 3a), it was found that the most significant uptake was obtained for Fe^{2+} (52%). This was followed by Mn^{2+}, Mg^{2+}, and Ca^{2+}, which concluded that the COF showed better affinity towards divalent cations than monovalent, and the presence of other ions interferes slightly with iron's adsorption. For **TAPB-DHTA-COF** (Fig. 3b), the removal rate achieved towards iron was also the highest, up to 84%. Iron adsorption practically did not decrease compared to the retention obtained in solutions only containing this metal. This material also interacted better with divalent ions than monovalent ones.

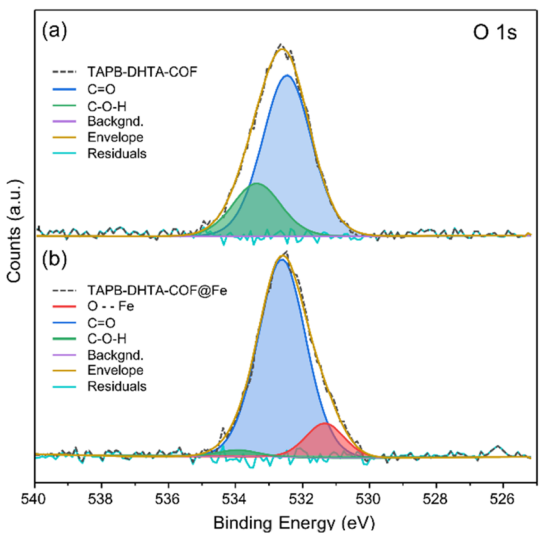

Fig. 4 XPS data for O 1s core level spectra of (a) the pristine TAPB-DHTA-COF and (b) TAPB-DHTA-COF@Fe, including a line shape analysis and deconvolution of the peaks.

Adsorption mechanism

To study the binding mechanism of Fe^{2+}, X-ray photoelectron spectroscopy (XPS) measurements were performed. For this study, only **TAPB-DHTA-COF** was explored. As it contains oxygen, any interaction between the –OH pendant groups from the pores and the Fe^{2+} ion can be followed by high-resolution XPS spectra acquisition of the O 1s core level. The COF was in contact for 3 h with a solution containing 20 ppm of Fe^{2+}. Later, the materials were recovered, air-dried, and activated with vacuum at 393 K before the XPS measurements. A survey spectrum of **TAPB-DHTA-COF** before and after the water treatment was performed, followed by a high-resolution XPS spectra acquisition.

In the XPS survey spectra of **TAPB-DHTA-COF@Fe** (see S11 from ESI†), the iron signal appeared at around 720 eV, compared to its absence in the pristine material. The Fe 2p signal indicated the presence of iron on the surface of the sample. Fig. S11.2 from ESI† shows the high-resolution spectra of the Fe 2p core level, a line shape analysis, and the deconvolution of the signal in the corresponding multiplets.[49] O 1s core level analysis for **TAPB-DHTA-COF** showed the peak could be deconvoluted into two components (Fig. 4). First, a significant contribution attributed to residual aldehyde C=O and a second one corresponding to the hydroxy functional groups in the pores C–O–H. After iron adsorption, a new contribution appeared in the XPS spectrum, attributed to the O–Fe interaction. Also, the signal of the C–O–H component had almost disappeared, which could only mean the hydroxy groups are the active sites of the COF.

Conclusions

In summary, two imine-based COF gels, **TAPB-PDA-GCOF** and **TAPB-DHTA-GCOF**, have been successfully synthesized at room

temperature. This approach is not only straightforward but also significantly reduces production time, energy, and economic costs from industrial preparation. The materials prepared in the form of gels, xerogels, and composite beads were used to remove Fe^{2+} from contaminated water. The adsorption properties of the developed materials for Fe^{2+} removal in waters were extensively explored. They were obtaining outstanding retention rates within very short contact times for the xerogels. The adsorption mechanism was studied *via* XPS, indicating the hydroxy groups of **TAPB-DHTA-COF** act as active sites inside the pores. Besides, the processed COF@PSU composite beads resulted in a product that can be directly employed in water treatment processes, showing an environmentally friendly alternative to the benchmark chemicals used in the water treatment industry.

This work suggests the potential of using imine-based COF gels for water remediation and paves the way for their use and manufacturing in commercial applications.

Author contributions

CRediT (Contributor Roles Taxonomy) was used for standardized contribution descriptions: C. Arqueros: data curation, formal analysis, investigation, methodology, validation, visualization, writing (original draft), writing (review & editing). C. Montoro: conceptualization, supervision, project administration, writing (review & editing). F. Zamora: conceptualization, supervision, project administration, resources, funding acquisition, writing (review & editing). L. Welte: conceptualization, supervision, resources, funding acquisition, writing (review & editing).

Conflicts of interest

There are no conflicts to declare.

Acknowledgements

We thank the financial support to the Spanish MICINN (PID2022-138908NB-C31, PDC2022-133498-I00 and TED2021-129886B-C42) and through the "María de Maeztu" Programme for Units of Excellence in R&D (CEX2023-001316-M). This work was also supported by the Comunidad de Madrid (MAD2D-CM-UAM, and IND2020/IND-17321) and MICINN (Planes complementarios, Materiales Avanzados). F. Z. also acknowledges support from the European Innovation Council under grant Agreement 101047081 (EVA).

Notes and references

1 I. Shiklomanov, in *Water in Crisis: A Guide to the World's Fresh Water Resources*, ed. P. H. Gleick, Oxford University Press, New York, 1993.
2 European Commission, The European Green Deal, **https://commission.europa.eu/strategy-and-policy/priorities-2019-2024/european-green-deal_es**, accessed 18 December 2023.
3 X. Xu, S. Liu, K. Smith, Y. Cui and Z. Wang, *J. Cleaner Prod.*, 2020, **276**, 124079.
4 F. Yang, B. Shi, J. Gu, D. Wang and M. Yang, *Water Res.*, 2012, **46**, 5423–5433.
5 2020/2184 Of The European Parliament And Of The Council of 16 December 2020, on the quality of water intended for human consumption, Directive (EU), 2015, **http://data.europa.eu/eli/dir/2020/2184/oj**.
6 World Health Organization (WHO), Health criteria and other supporting information, *Guidelines for Drinking-Water Quality*, World Health Organization, Geneva, 2nd edn, 1996, vol. 2.
7 R. A. Barakwan, A. R. Syavira and Y. Trihadiningrum, *IOP Conf. Ser. Earth Environ. Sci.*, 2020, **506**, 012009.
8 Y. Liu and P. Zhang, *Polymers*, 2022, **14**, 2673–2700.
9 E. A. Gendy, J. Ifthikar, J. Ali, D. T. Oyekunle, Z. Elkhlifia, I. I. Shahib, A. I. Khodair and Z. Chen, *J. Environ. Chem. Eng.*, 2021, **9**, 105687.
10 I. T. Y. Lam, S.-J. Choi, D. Lu and Y. Kim, *Nanoscale*, 2023, **15**, 10189–10205.
11 Z. Wang, S. Zhang, Y. Chen, Z. Zhang and S. Ma, *Chem. Soc. Rev.*, 2020, **49**, 708–735.
12 F. J. Uribe-Romo, J. R. Hunt, H. Furukawa, C. Klöck, M. O'Keeffe and O. M. Yaghi, *J. Am. Chem. Soc.*, 2009, **131**, 4570–4571.
13 A. Halder, S. Karak, M. Addicoat, S. Bera, A. Chakraborty, S. H. Kunjattu, P. Pachfule, T. Heine and R. Banerjee, *Angew. Chem., Int. Ed.*, 2018, **57**, 5797–5802.
14 J. Gan, X. Li, K. Rizwan, M. Adeel, M. Bilal, T. Rasheed and H. M. N. Iqbal, *Chemosphere*, 2022, **286**, 131710.
15 Y. Liang, L. Feng, X. Liu, Y. Zhao, Q. Chen, Z. Sui and N. Wang, *Chem. Eng. J.*, 2021, **404**, 127095.
16 Y. Tang, H. Huang, W. Xue, Y. Chang, Y. Li, X. Guo and C. Zhong, *Chem. Eng. J.*, 2020, **384**, 123382.
17 S. Zhuang, R. Chen, Y. Liu and J. Wang, *J. Hazard. Mater.*, 2020, **385**, 121596.
18 X. Zhu, S. An, Y. Liu, J. Hu, H. Liu, C. Tian, S. Dai, X. Yang, H. Wang, C. W. Abney and S. Dai, *AIChE J.*, 2017, **63**, 3470–3478.
19 F. Pan, W. Guo, Y. Su, N. A. Khan, H. Yang and Z. Jiang, *Sep. Purif. Technol.*, 2019, **215**, 582–589.
20 A. Guillem-Navajas, J. Á. Martín-Illán, E. Salagre, E. G. Michel, D. Rodriguez-San-Miguel and F. Zamora, *ACS Appl. Mater. Interfaces*, 2022, **14**, 50163–50170.
21 W. R. Cui, W. Jiang, C. R. Zhang, R. P. Liang, J. Liu and J. D. Qiu, *ACS Sustain. Chem. Eng.*, 2019, **8**, 445–451.
22 L. Wang, H. Xu, Y. Qiu, X. Liu, W. Huang, N. Yan and Z. Qu, *J. Hazard. Mater.*, 2020, **389**, 121824.
23 L. Merí-Bofí, S. Royuela, F. Zamora, M. L. Ruiz-González, J. L. Segura, R. Muñoz-Olivas and M. J. Mancheño, *J. Mater. Chem. A*, 2017, **5**, 17973–17981.
24 X.-F. Lu, W.-H. Ji, L. Yuan, S. Yu and D.-S. Guo, *Ind. Eng. Chem. Res.*, 2019, **58**, 17660–17667.
25 T. Xu, L. Zhou, Y. He, S. An, C. Peng, J. Hu and H. Liu, *Ind. Eng. Chem. Res.*, 2019, **58**, 19642–19648.
26 J. Á. Martín-Illán, D. Rodríguez-San-Miguel and F. Zamora, *Coord. Chem. Rev.*, 2023, **495**, 215342.

27 Y. Zhang, H. Wang, W. Wang, Z. Zhou, J. Huang, F. Yang, Y. Bai, P. Sun, J. Ma, L. E. Peng, C. Y. Tang and L. Shao, *Matter*, 2024, **7**, 1406–1439.
28 J. Á. Martín-Illán, D. Rodríguez-San-Miguel, O. Castillo, G. Beobide, J. Perez-Carvajal, I. Imaz, D. Maspoch and F. Zamora, *Angew. Chem., Int. Ed.*, 2021, **60**, 13969–13977.
29 J. Á. Martín-Illán, J. A. Suárez, J. Gómez-Herrero, P. Ares, D. Gallego-Fuente, Y. Cheng, D. Zhao, D. Maspoch and F. Zamora, *Adv. Sci.*, 2022, **9**, 2104643.
30 S. Royuela, S. Sevim, G. Hernanz, D. Rodríguez-San-Miguel, P. Fischer, C. Franco, S. Pané, J. Puigmartí-Luis and F. Zamora, *Adv. Funct. Mater.*, 2023, **34**, 2314634.
31 C. H. Feriante, S. Jhulki, A. M. Evans, R. R. Dasari, K. Slicker, W. R. Dichtel and S. R. Marder, *Adv. Mater.*, 2020, **32**, 1905776.
32 D. Zhu, Y. Zhu, Q. Yan, M. Barnes, F. Liu, P. Yu, C.-P. Tseng, N. Tjahjono, P.-C. Huang, M. M. Rahman, E. Egap, P. M. Ajayan and R. Verduzco, *Chem. Mater.*, 2021, **33**, 4216–4224.
33 F. G. Fabozzi, N. Severin, J. P. Rabe and S. Hecht, *J. Am. Chem. Soc.*, 2023, **145**, 18205–18209.
34 Z. Liu, K. Zhang, G. Huang, B. Xu, Y. Hong, X. Wu, Y. Nishiyama, S. Horike, G. Zhang and S. Kitagawa, *Angew. Chem., Int. Ed.*, 2022, **61**, e202110695.
35 G. Boix, X. Han, I. Imaz and D. Maspoch, *ACS Appl. Mater. Interfaces*, 2021, **13**, 17835–17843.
36 B. Valizadeh, T. N. Nguyen, B. Smit and K. C. Stylianou, *Adv. Funct. Mater.*, 2018, **28**, 1801596.
37 H. Woo and H. Li, *Advanced Functional Materials*, Springer, Berlin, Heidelberg, 2011.
38 S. Azizian and S. Eris, in *Adsorption: Fundamental Processes and Applications*, ed. M. Ghaedi, Elsevier, 2021, vol. 33, pp. 445–509.
39 S. S. Ray, R. Gusain and N. Kumar, in *Carbon Nanomaterial-Based Adsorbents for Water Purification*, ed. S. S. Ray, R. Gusain and N. Kumar, Elsevier, 2020, pp. 101–118.
40 A. bin Jusoh, W. H. Cheng, W. M. Low, A. Nora'aini and M. J. Megat Mohd Noor, *Desalination*, 2005, **182**, 347–353.
41 M. A. Akl, A. M. Yousef and S. AbdElnasser, *J. Chem. Eng. Process Technol.*, 2013, **4**, 1–10.
42 M. A. Shavandi, Z. Haddadian, M. H. S. Ismail, N. Abdullah and Z. Z. Abidin, *J. Taiwan Inst. Chem. Eng.*, 2012, **43**, 750–759.
43 D. Dutta, R. Dubey, S. Banerjee, J. P. Borah and A. Puzari, *Environ. Challenges*, 2021, **4**, 100115.
44 J. P. Vistuba, M. E. Nagel-Hassemer, F. R. Lapolli and M. Á. Lobo Recio, *Environ. Technol.*, 2013, **34**, 275–282.
45 S. S. Tahir and N. Rauf, *J. Environ. Manage.*, 2004, **73**, 285–292.
46 H. Yan, H. Li, X. Tao, K. Li, H. Yang, A. Li, S. Xiao and R. Cheng, *ACS Appl. Mater. Interfaces*, 2014, **6**, 9871–9880.
47 Y. Xiao, C. Ma, Z. Jin, J. Wang, L. He, X. Mu, L. Song and Y. Hu, *Chem. Eng. J.*, 2021, **421**, 127837.
48 Z. A. Ghazi, A. M. Khattak, R. Iqbal, R. Ahmad, A. A. Khan, M. Usman, F. Nawaz, W. Ali, Z. Felegari, S. U. Jan, A. Iqbal and A. Ahmad, *New J. Chem.*, 2018, **42**, 10234–10242.
49 T. Yamashita and P. Hayes, *Appl. Surf. Sci.*, 2008, **254**, 2441–2449.

